On the nature of the singlet and triplet excitations mediating thermally activated delayed fluorescence.

Y. Olivier,[1] B. Yurash,[2] L. Muccioli,[3] G. D'Avino,[4] O. Mikhnenko,[2] J.C. Sancho-García,[5] C. Adachi,[6] T.-Q. Nguyen[2] and D. Beljonne[1]

[1]Laboratory for Chemistry of Novel Materials, University of Mons-Hainaut, Place du Parc 20, B-7000 Mons, Belgium.

[2]Department of Chemistry and Biochemistry, Center for Polymers and Organic Solids, University of California, Santa Barbara, CA, United States

[3]Dipartimento di Chimica Industriale "Toso Montanari",Università di Bologna, Bologna, Italy, and Institut des Sciences Moléculaires, UMR 5255, University of Bordeaux, Talence, France.

[4]Grenoble Alpes University, CNRS, Institut Néel, F-38042 Grenoble, France.

[5]Departamento de Química Física, Universidad de Alicante, E-03080 Alicante, Spain.

[6]Center for Organic Photonics and Electronics Research (OPERA) Kyushu University 744 Motooka, Nishi, Fukuoka 819-0395, Japan

Table of contents

Section 1: Supplementary materials and computational details

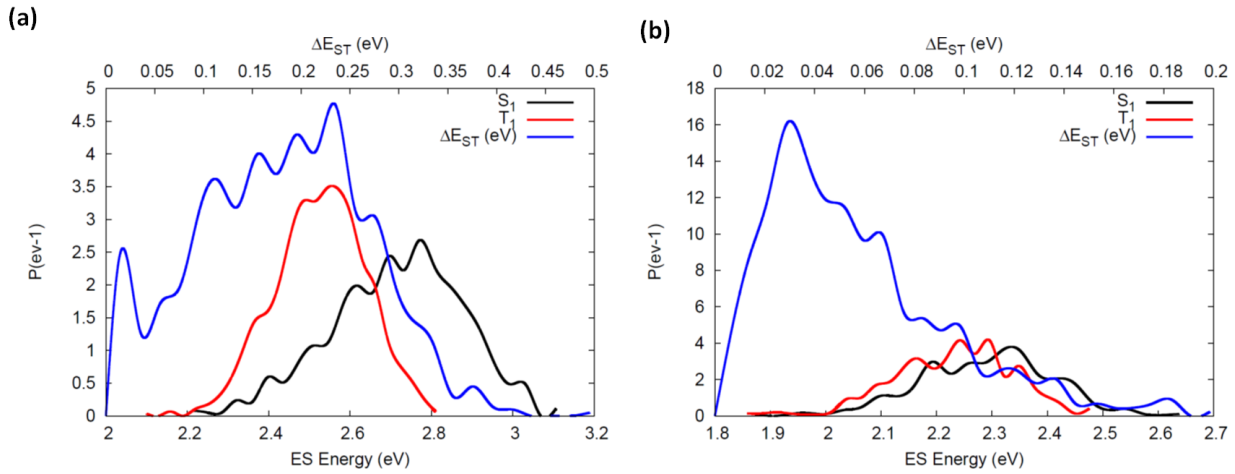

Figure S1: Lowest energy singlet (black) and triplet (red) as well as a singlet-triplet energy gap (blue) distributions calculated at the TDA-PBE0 level using 6-31G(d,p) basis set for **a)** 2CzPN and **b)** 4CzIPN.

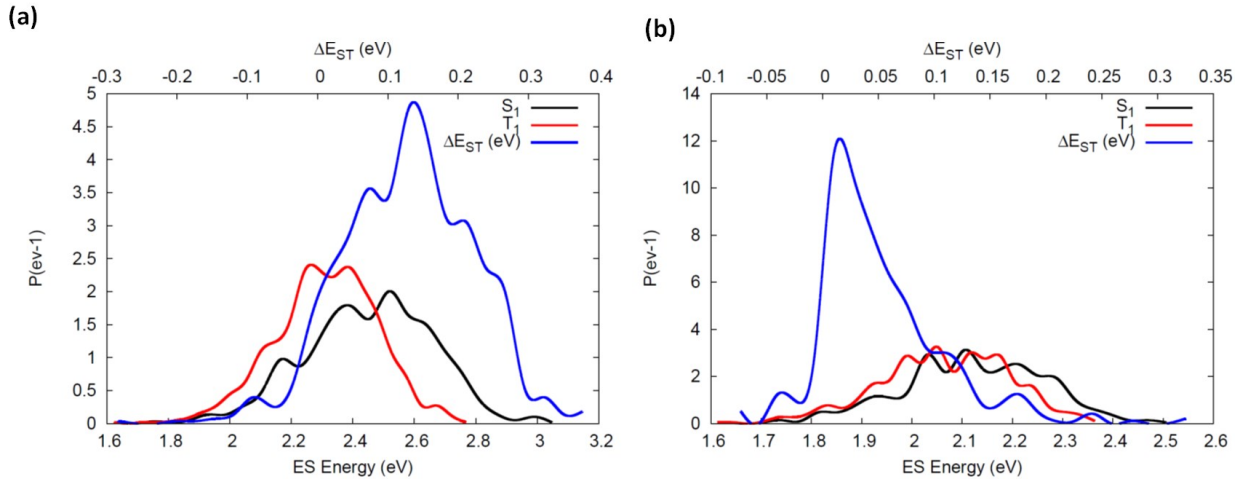

Figure S2: Lowest singlet (black) and triplet (red) as well as a singlet-triplet energy gap (blue) calculated at the TDA-PBE0 level using 6-31G(d,p) basis set coupled to microelectrostatic calculations for **a)** 2CzPN and **b)** 4CzIPN.

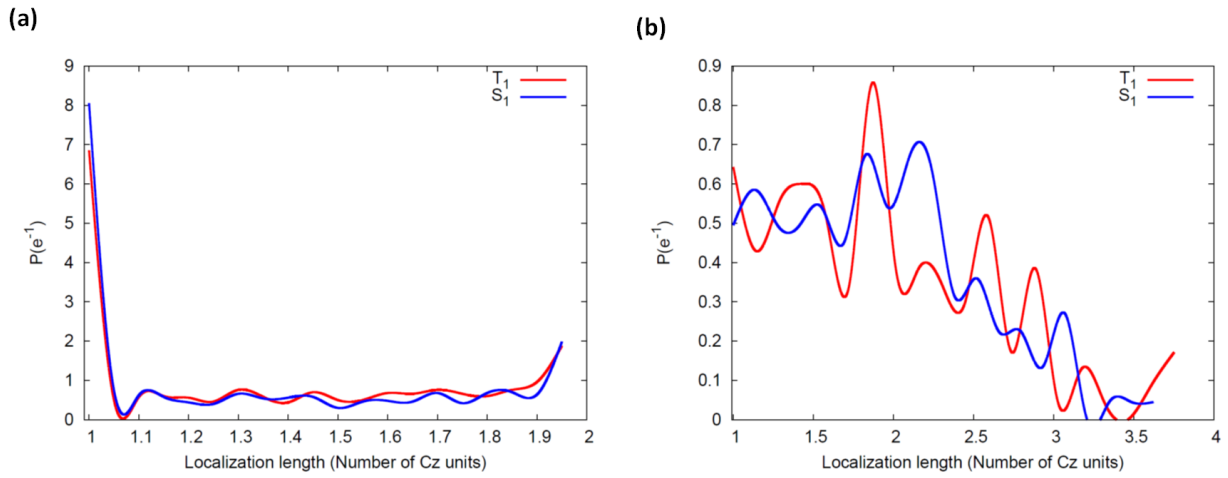

Figure S3: Localization lengths in number of carbazole units (Inverse participation ratios) calculated on the basis of changes in ESP (Electro Static Potential) charges between the ground and excited states for the lowest singlet (blue) and triplet excited states (red) for **a)** 2CzPN and **b)** 4CzIPN.

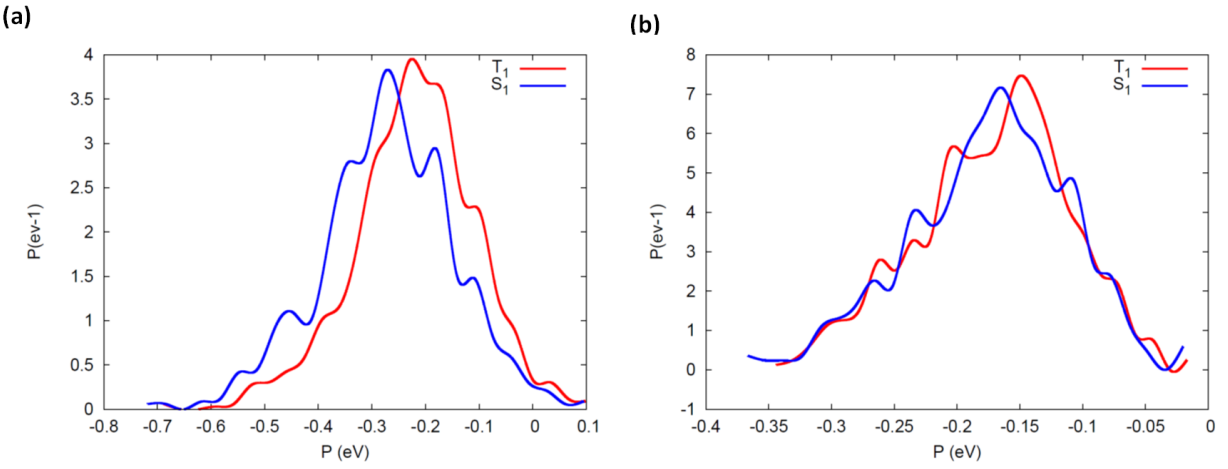

Figure S4: Distribution of total polarization energy as obtained from microelectrostatic calculations for the lowest singlet (blue) and triplet (red) excited states for **a)** 2CzPN and **b)** 4CzIPN.

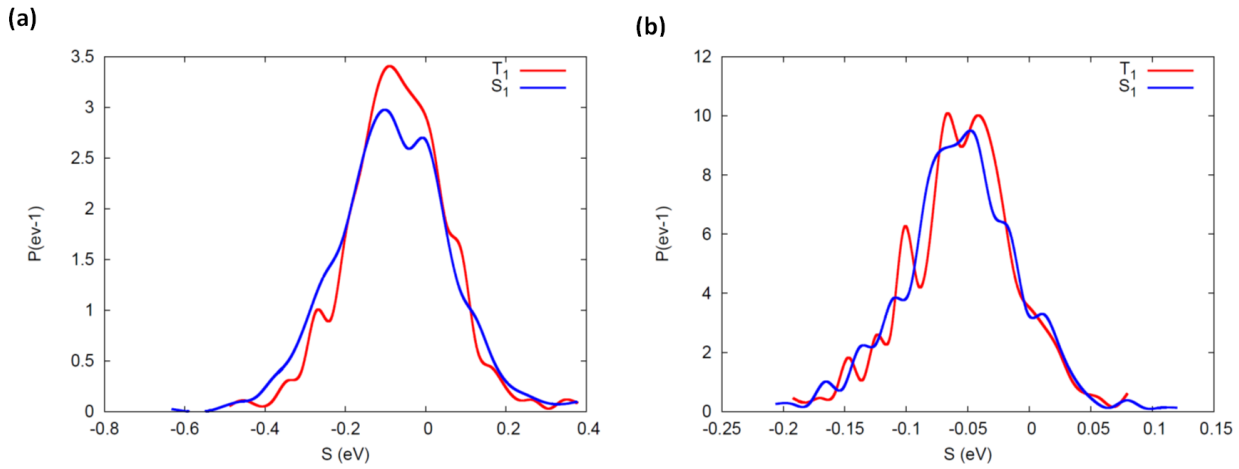

Figure S5: Distribution of the electrostatic contribution to the total polarization energy as obtained from microelectrostatic calculations for the lowest singlet (blue) and triplet (red) excited states for **a)** 2CzPN and **b)** 4CzIPN.

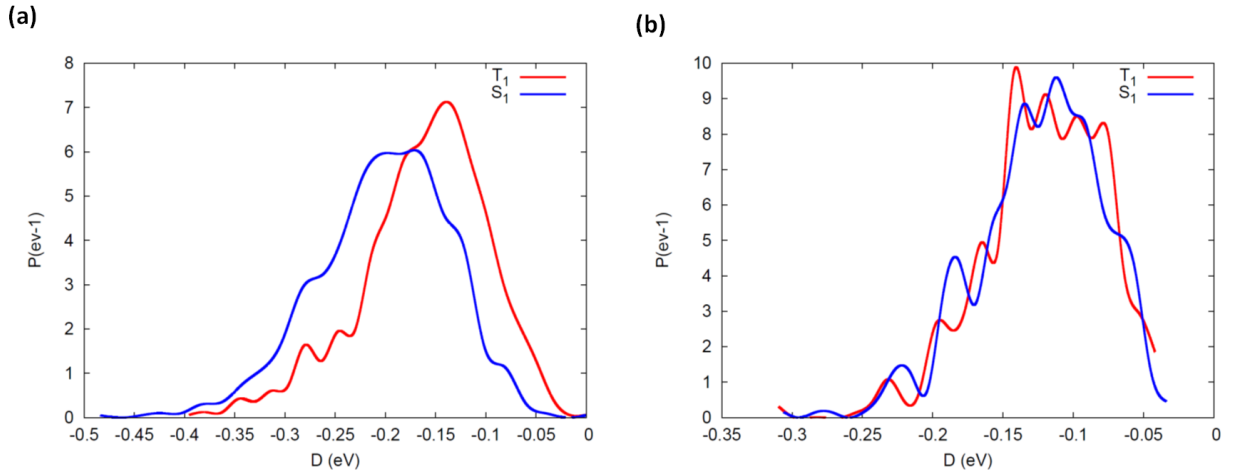

Figure S6: Distribution of the induction contribution to the total polarization energy as obtained from microelectrostatic calculations for the lowest singlet (blue) and triplet (red) excited states for **a)** 2CzPN and **b)** 4CzIPN.

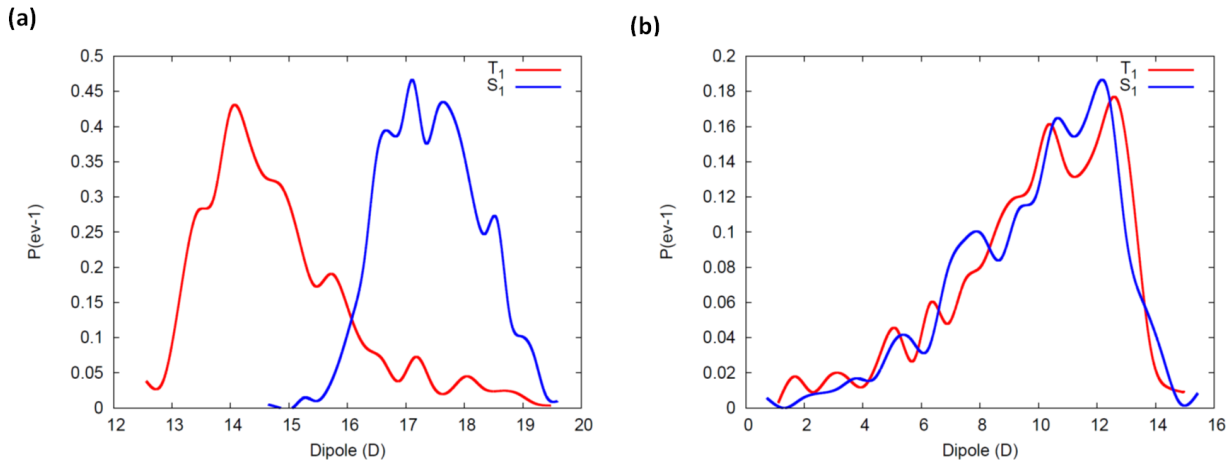

Figure S7: Electric dipole distribution calculated at TDA-PBE0/6-31G(d,p) level in the lowest singlet (blue) and triplet (red) exited states for **a)** 2CzPN and **b)** 4CzIPN.

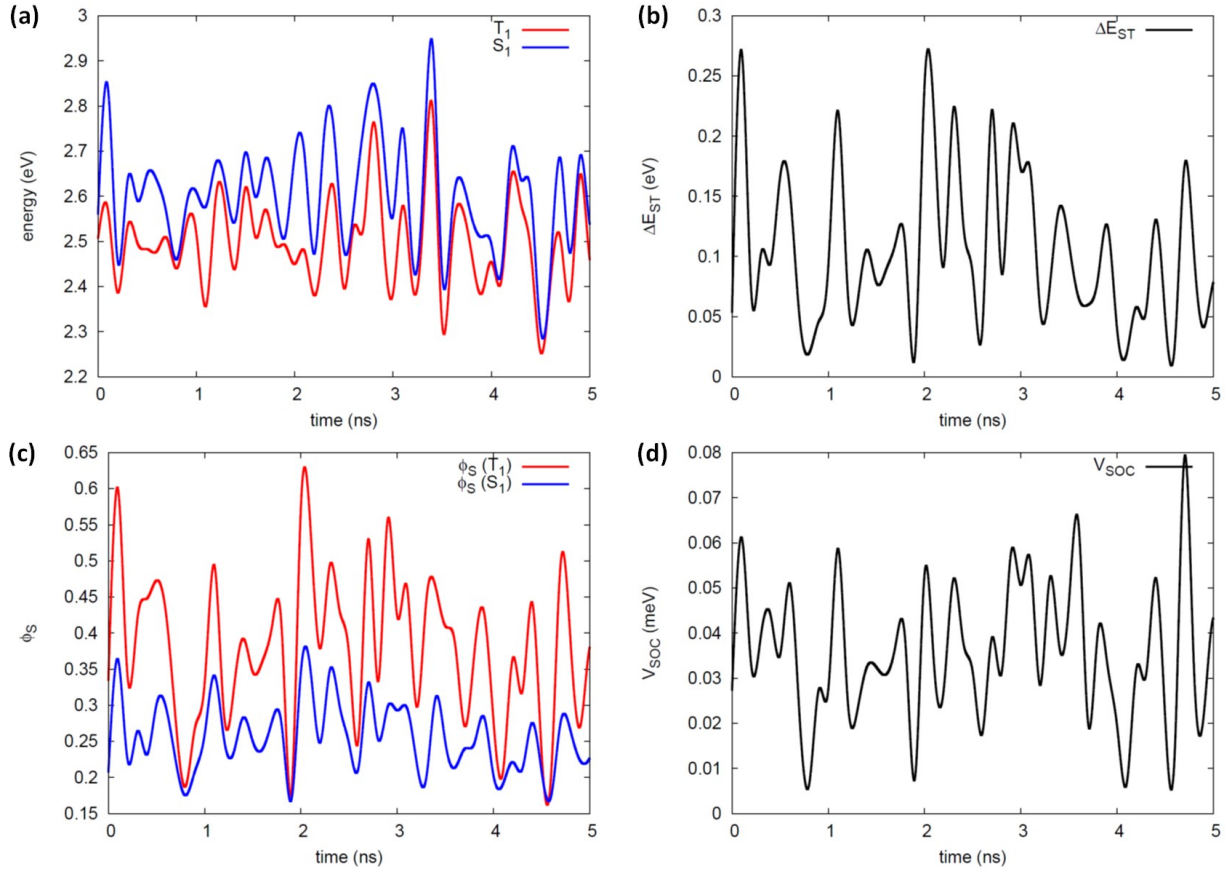

Figure S8: Time evolution of electronic parameters for one specific 2CzPN molecule along the MD trajectory: **(a)** T_1, S_1 energies and **(b)** ΔE_{ST} calculated at the TDA-PBE0/6-31G(d,p); **(c)** $\phi_S(T_1)$ and $\phi_S(S_1)$; and **(d)** S_1-T_1 spin-orbit coupling calculated at the PBE0/DZ using the scalar relativistic ZORA method.

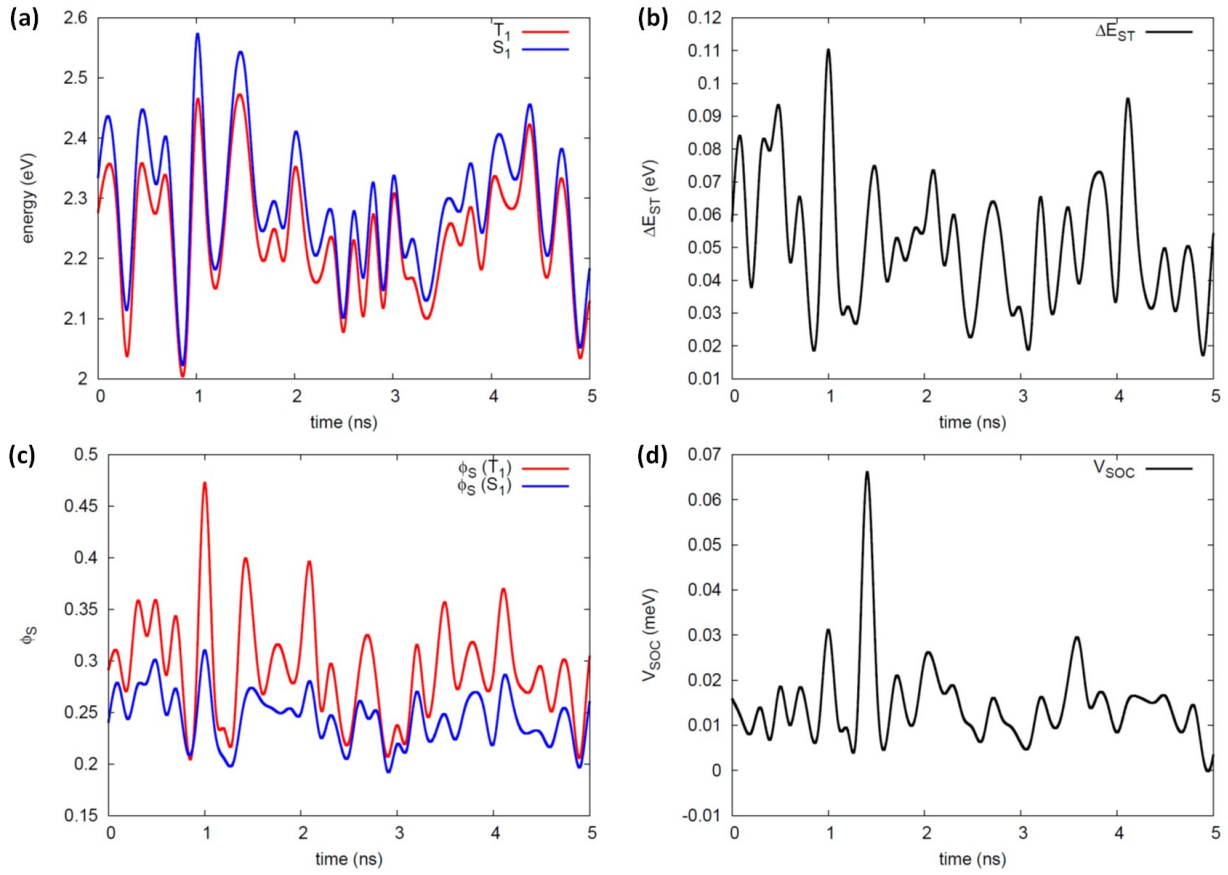

Time evolution of electronic parameters for one specific 4CzIPN molecule along the MD trajectory: **(a)** T_1, S_1 energies and **(b)** ΔE_{ST} calculated at the TDA-PBE0/6-31G(d,p); **(c)** $\phi_S(T_1)$ and $\phi_S(S_1)$; and **(d)** S_1-T_1 spin-orbit coupling calculated at the PBE0/DZ using the scalar relativistic ZORA method.

	TDA			**TDA + ME**		
	T_1 (eV)	**S_1 (eV)**	**ΔE_{ST} (eV)**	**T_1 (eV)**	**S_1 (eV)**	**ΔE_{ST} (eV)**
2CzPN	2.54±0.11	2.73±0.16	0.19±0.09	2.34±0.17	2.48±0.21	0.14±0.09
4CzIPN	2.24±0.11	2.32±0.12	0.06±0.04	2.08±0.13	2.14±0.14	0.06±0.06

Table S1: Average T_1, S_1 and ΔE_{ST} values as calculated at the TDA-PBE0/6-31G(d,p) level, and coupled to ME calculations.

Molecular dynamics simulation computational details

We have performed 100 ns MD simulations on samples of 1000 2CzPN and 580 4CzIPN molecules using a validated united atom force field [1] by slowly decreasing the external pressure and the temperature from an initial structure generated at high pressure (1000 atm) and high temperature (1000 K). After equilibration at 300 K, the calculated densities amount to 1.19 g/cm³ and 1.15 g/cm³ for 2CzPN and 4CzIPN respectively, in reasonable agreement with experiments (1.32 g/cm³ for 2CzPN and 1.12 g/cm³ for 4CzIPN).

Excited state energy calculations based on MD geometries

All the Time-Dependent Density Functional excited calculations have been performed within the Tamm-Dancoff Approximation (TDA-DFT) using the hybrid PBE0 functional [2] and the 6-31G(d,p) basis set on single molecule geometries extracted along the MD runs, as previously validated. [3]

Microelectrostatic calculations methodology

Because of their partial CT character, one can anticipate that singlet and triplet excitation energies in the 2CzPN (and 4CzIPN) bulk are sensitive to solid-state electronic polarization effects, with a differential that directly reflects the relative magnitude of the CT contribution to their wavefunctions. Here, we adopt an atomistic ME scheme where excited molecules are embedded in a dielectric environment described as a set of classical point charges and anisotropic polarizabilities, accounting for both electrostatic (ΔS) and induction (ΔI) contributions. The polarization energy (P=ΔS+ΔI) quantifies the environmental contribution to S_1 and T_1 energies. P is assessed by performing self-consistent ME calculations on large around each individual molecule (spheres of 40 Å radius provided convergent results). For each calculation, a state and conformation-dependent set of atomic ESP charges is assigned to the molecular geometries explored along the MD trajectories, while all the polarizabilities are taken from ground-state calculations on the optimized Molecular Mechanics geometry. All simulations are performed at the PBE0 level with the 6-311G(d,p) basis set.

Spin-orbit calculations methodology

All V_{SOC} matrix elements between S_1 and T_1 have been computed by applying the zeroth order regular approximation (ZORA) [4–6] to the full Breit-Dirac relativistic equation at the PBE0/Double Zeta polarized level.

Since the (R)ISC rate constant is proportional to the square of the S_1-T_1 V_{SOC}, contributions from $T_{1,x}$, $T_{1,y}$ and $T_{1,z}$ sublevels have to be taken into account. In this study, V_{SOC} are presented as the root sum square of the spin-orbit coupling integrals from all three triplet sublevels : [6]

$$V_{SOC} = \langle S_1|H_{SO}|T_1\rangle = \sum_{\alpha=x,y,z} \left[\left(Re\langle S_1|H_{SO}|T_{1,\alpha}\rangle\right)^2 + \left(Im\langle S_1|H_{SO}|T_{1,\alpha}\rangle\right)^2\right]^{\frac{1}{2}} \quad (S1)$$

where *Re* and *Im* stand for real and imaginary parts, respectively.

	$\lvert V_{SOC}\rvert$ (meV)	$\sigma_{V_{SOC}}$ (meV)	$\sqrt{\lvert V_{SOC}^2\rvert}$ (meV)
2CzPN	0.039	0.019	0.054
4CzIPN	0.015	0.008	0.02

Table S2: Average, standard deviation and thermally averaged spin-orbit coupling calculated at the PBE0/DZP level applying the zeroth order regular approximation to full Breit-Dirac relativistic equation.

	$\sigma_{S_1}^{stat}$ (eV)	$\sigma_{S_1}^{dyn}$ (eV)	$\sigma_{S_1}^{tot}$ (eV)	$\sigma_{T_1}^{stat}$ (eV)	$\sigma_{T_1}^{dyn}$ (eV)	$\sigma_{T_1}^{tot}$ (eV)	$\sigma_{\Delta E_{ST}}^{stat}$ (eV)	$\sigma_{\Delta E_{ST}}^{dyn}$ (eV)	$\sigma_{\Delta E_{ST}}^{tot}$ (eV)
2CzPN	0.07	0.12	0.14	0.04	0.10	0.11	0.039	0.068	0.078
4CzIPN	0.04	0.11	0.12	0.03	0.10	0.11	0.015	0.026	0.030

Table S3: Static (stat), dynamic (dyn) contributions to the total (tot) energetic disorder of the polarization energy for lowest singlet (S_1) and triplet (T_1) excited and singlet-triplet energy difference (ΔE_{ST}).

Static and dynamic disorders evaluation

We consider a physical observable *A* calculated for *N* molecules along an MD trajectory.

The standard deviation of the static disorder $\sigma_{\mathrm{A}}^{stat}$ for this observable can be expressed as:

$$\sigma_{\mathrm{A}}^{stat} = \sqrt{\frac{\sum_n (\bar{A}_n - \bar{A})^2}{N}} \qquad (S2)$$

Where the sum runs over the number of molecules, $\bar{A}_n$ is the average calculated along the molecular dynamics trajectory of the observable *A* calculated for molecule *n*, $\bar{A}$ is the average over both the set of *N* molecules and the *I* configurations of the MD trajectory.

The standard deviation of the dynamic disorder $\sigma_{\mathrm{A}}^{dyn}$ for this observable can be expressed as:

$$\sigma_{\mathrm{A}}^{dyn} = \sqrt{\frac{\sum_i \sum_n \left(A_{n,i} - \bar{A}_n\right)^2}{NI}} \qquad (S3)$$

Where the sum runs over both the set of *N* molecules and the *I* snapshots and $A_{n,i}$ is the value of for molecule *n* at snapshots *i*.

Accounting for polaronic effects on the spin-orbit coupling (V_{SOC}) and the rate of (reverse) intersystem crossing ($k_{(R)ISC}$) evaluation for 4CzIPN.

(R)ISC process occurs from the relaxed S_1 (T_1) states. Practically speaking, estimating the $k_{(R)ISC}$ would require to calculate optimize V_{SOC} in the relaxed S_1 and T_1 excited states geometries within the simulated amorphous films. However, this is computationally unfeasible, and in a first attempt to account for polaronic effects, we have thus calculated V_{SOC} from the optimized gas phase S_1 and T_1 excited states geometries.

	V_{SOC} (meV)		
	S_0	**S_1**	**T_1**
4CzIPN	0.030	0.015	0.023

Table S2: Spin-orbit coupling calculation with PBE0 functional and DZ basis set using the scalar relativistic ZORA method starting from the optimized S_0 (ground state), S_1 and T_1 gas phase geometries.

V_{SOC} obtained for both S_1 and T_1 appears to be smaller than V_{SOC} obtained for the ground state optimized geometry. We thus renormalize the V_{SOC} used to compute $k_{(R)ISC}$ by the ratio of V_{SOC} (S_1)/V_{SOC} (S_0) (V_{SOC} (T_1)/V_{SOC} (S_0) so that $k_{(R)ISC}^{corr}$ reported in Table 2 writes:

$$k_{RISC}^{corr} = k_{RISC} \times \left[\frac{V_{SOC}(S_1)}{V_{SOC}(S_0)}\right]^2 \quad (S4)$$

$$k_{ISC}^{corr} = k_{ISC} \times \left[\frac{V_{SOC}(T_1)}{V_{SOC}(S_0)}\right]^2 \quad (S5)$$

where the states between parentheses indicate the relaxed geometry employed in the calculation.

Ground state polarisabilities

	α_{xx} (Å^3)	α_{xy} (Å^3)	α_{xz} (Å^3)	α_{yy} (Å^3)	α_{yz} (Å^3)	α_{zz} (Å^3)
2CzPN	63.78	0.07	-0.07	50.38	13.54	50.49
4CzIPN	100.23	-2.07 x 10^{-3}	-2.52 x 10^{-3}	94.63	13.39	96.54

Table S3: Ground state polarisabilities calculated at the PBE0/6-311G(d,p) level.

Section 2: Materials and experimental details

Methods and Materials

4CzIPN and 2CzPN were synthesized and purified according to the general procedure originally described in reference [7]. Thin films of approximately 100 nm thickness were made on glass substrates in an inert environment by spin-coating from solution (700 rpm, 10 mg/mL in chloroform). Samples were either encapsulated using epoxy resin and another glass substrate, or placed inside of a liquid nitrogen-cooled cryostat (also used for temperature dependent measurements) in order to maintain an oxygen-free environment during photoluminescence (PL) measurements. PL lifetime measurements were carried out using a Time-Correlated Single Photon Counting technique. Samples were excited at 400 nm using a Ti:Sapphire laser with an approximately 200 fs pulse width. For all measurements the intensity of the laser was attenuated such that each pulse produced fewer than 3×10^{11} excitons per cm^2, well below the threshold for exciton-exciton annihilation. The solid-state density of 4CzIPN and 2CzPN in neat films is 1.12 and 1.32 g cm^{-3}, respectively, as determined by X-Ray Reflectivity.

Molar Absorptivity

The molar absorptivity of 2CzPN and 4CzIPN in the solid-state was determined by the absorption spectra of thin films of accurately known thickness, as determined by a profilometer.

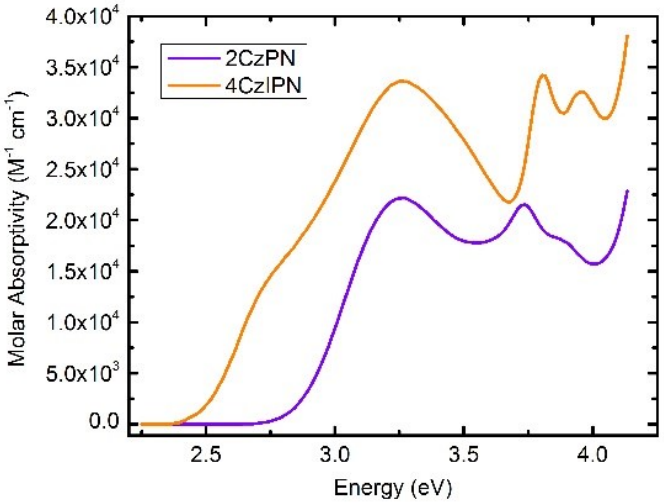

Figure S10: Molar Absorptivity of 2CzPN and 4CzIPN.

Photoluminescence (PL) Spectra

PL spectra were obtained using a 400 nm continuous-wave diode laser and a CCD camera.

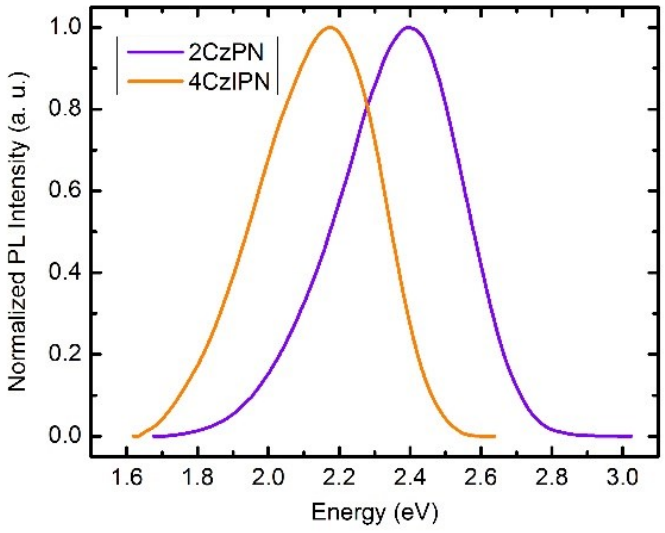

Figure S11: PL spectra of 2CzPN and 4CzIPN.

Quantum Yield of 4CzIPN

The total photoluminescence quantum yield of thin films, ϕ_{total}, was obtained through the use of an integrating sphere and a 400 nm continuous wave diode laser. At room temperature ϕ_{total} was determined to be 30.3% and 37.5% for 4CzIPN and 2CzPN, respectively. The steady-state PL spectrum was measured (at constant excitation power using a 400 nm continuous wave diode laser) at various temperatures and then integrated in order to estimate the temperature dependence of the total quantum yield. ϕ_{total} is given by the sum of the prompt (ϕ_p) and delayed (ϕ_d) photoluminescence quantum yields:

$$\Phi_{total} = \Phi_p + \Phi_d \qquad (S6)$$

The quantum yields of the prompt and delayed components were determined at various temperatures according to:

$$\Phi_p = \Phi_{total} \times \frac{A_p\tau_p}{A_p\tau_p + A_d\tau_d} \qquad (S7)$$

$$\Phi_d = \Phi_{total} \times \frac{A_d\tau_d}{A_p\tau_p + A_d\tau_d} \qquad (S8)$$

where τ_p and τ_d are equivalent to the reciprocal of k_p and k_d, respectively, and A_p and A_d are the relative amplitudes of the prompt and delayed components, respectively. These parameters are obtained upon

fitting the PL decay at a given temperature to Equation S11 (*vide infra*). The temperature dependent quantum yield (total, prompt, and delayed) of 4CzIPN is shown in Figure S12.

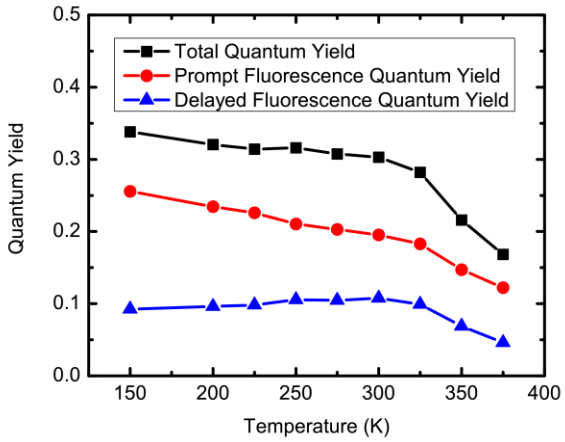

Figure S12: Temperature dependence of the quantum yield of 4CzIPN.

Analytical Model

The rates of ISC and RISC were assessed by comparing the neat photoluminescence (PL) decay of a 4CzIPN film with that predicted by an analytical model which describes the interplay of all of the photophysical processes that occur in TADF materials. [8,9] A kinetic scheme showing these processes is presented in Figure S13.

The differential rate laws for the decay of singlets (S_1) and triplets (T_1) are given by Equations S9 and S10, respectively:

$$\frac{-d[S_1]}{dt} = k^S[S_1] - k_{RISC}[T_1] = (k_{nr}^S + k_r^S + k_{ISC})[S_1] - k_{RISC}[T_1] \quad (S9)$$

$$\frac{-d[T_1]}{dt} = k^T[T_1] - k_{ISC}[S_1] = (k_{nr}^T + k_r^T + k_{RISC})[T_1] - k_{ISC}[S_1] \quad (S10)$$

Where k^S and k^T represent the sum of the rates for decay pathways that originate in the singlet state and triplet state, respectively; k_r^S is the fluorescence decay rate and k_r^T is the phosphorescence decay rate; k_{nr}^S and k_{nr}^T are the rates of non-radiative decay to the ground state via internal conversion from the singlet and triplet manifolds, respectively; and $k_{(R)ISC}$ is the rate of (reverse) intersystem crossing;

From the initial boundary condition that only singlets are directly excited, i.e. $[S_1]=[S_1]_0$ and $[T_1]=0$ when t=0, we find a solution for the PL decay of singlets given by:

$$[S_1] = A_p \exp(-k_p t) + A_d \exp(-k_d t) \quad (S11)$$

where A_p and A_d are the relative amplitudes of the prompt and delayed decay components, respectively, k_p is the rate of prompt fluorescence, and k_d is the rate of delayed fluorescence.

In terms of the rates of the individual photophysical processes described in Equations S9 and S10, we find that the rates of prompt and delayed fluorescence in Equation S11 are given by:

$$k_p = \frac{1}{2}\left\{(k^S + k^T) + \sqrt{(k^T - k^S)^2 + 4k_{ISC}k_{RISC}}\right\} \quad (S12)$$

$$k_d = \frac{1}{2}\left\{(k^S + k^T) - \sqrt{(k^T - k^S)^2 + 4k_{ISC}k_{RISC}}\right\} \quad (S13)$$

The expression for k_p can be greatly simplified when we consider the very different lifetimes of singlets and triplets. At short timescales (i.e. tens of nanoseconds) the dominating term in Equation S9 is $k^S[S_1]$, because $k_{RISC} << k^S$ and $[T_1] << [S_1]$. Thus, the differential rate law describing singlet decay at short timescales is given by:

$$\frac{-d[S_1]}{dt} \approx k^S[S_1] \quad (S14)$$

from which it follows that the time-dependent solution is:

$$[S_1] = A_p \exp(-k_p t) \quad (S15)$$

where $k_p \approx k^S$. Furthermore, it has been established in the literature that TADF materials have a very stable, long-lived triplet state whose lifetime is limited only by k_{RISC}. [10–12] Therefore, we take k_{nr}^T and k_r^T in Equation S10 to be negligible, resulting in $k^T \approx k_{RISC}$. Upon substitution of $k_p = k^S$ and $k_{RISC} = k^T$ into Equation S13 we obtain:

$$k_d = \frac{1}{2}\left\{(k_p + k_{RISC}) - \sqrt{(k_{RISC} - k_p)^2 + 4k_{ISC}k_{RISC}}\right\} \quad (S16)$$

and upon solving for k_{RISC} we find that:

$$k_{RISC} = \frac{k_d^2 - k_p k_d}{k_{ISC} + k_d - k_p} \quad (S17)$$

Using the theoretical value of 2.6×10^6 s^{-1} for k_{ISC} and the experimental values of k_p and k_d, we obtain from Equation S17 a value of 5.9×10^5 s^{-1} for k_{RISC}, which is very close to the theoretical value of 6.6×10^5 s^{-1} (see Table 2). In order to assess the validity of particular values of k_{ISC} and k_{RISC}, we calculated the theoretical PL decay (Equation S11) by using our experimental value for k_p and the theoretical value of k_d (see Table 2 main text). The calculated PL decay was then compared to the experimental PL decay, as shown in Figure 4a in the main text. This procedure was also done using the theoretical values uncorrected for polaronic effects (see Table 2) of 1.14×10^7 s^{-1} for k_{ISC} and 1.1×10^6 s^{-1} for k_{RISC}, but with these uncorrected values we find considerable disagreement with the experimental PL decay (see Figure S14).

In order to experimentally determine ΔE_{ST} in 4CzIPN, we first estimated the temperature dependence of reverse intersystem crossing using the equation previously developed by Berberan-Santos *et al.* [8] and adapted by Adachi: [13]

$$k_{RISC}(T) = \frac{k_p(T)k_d(T)}{k_{ISC}} \times \frac{\Phi_d(T)}{\Phi_p(T)} \quad (S18)$$

where k_{ISC} is assumed to be temperature independent, ϕ_d is the quantum yield of delayed fluorescence, and ϕ_p is the quantum yield of prompt fluorescence. The method used to determine the prompt and delayed quantum yields is described in the previous section. [26] k_p and k_d were obtained by fitting the PL decay of a pristine 4CzIPN film to Equation S11 and the theoretical value of 2.6×10^6 s^{-1} was used for k_{ISC}.

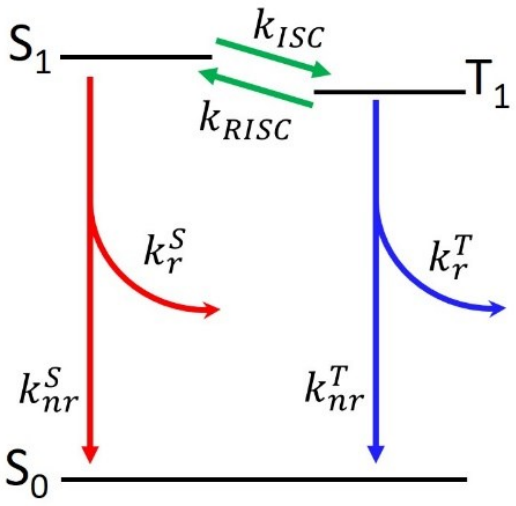

Figure S13: Simplified Jablonski diagram showing the relevant excited-state photophysical processes for TADF materials. S_1 and T_1 represent the lowest energy singlet and triplet excited states, respectively. k_{nr}^S and k_{nr}^T are the non-radiative rates of decay for singlets and triplets, respectively. k_r^S and k_r^T are the radiative rates of decay for singlets (fluorescence) and triplets (phosphorescence), respectively. k_{ISC} and k_{RISC} are the rates of intersystem crossing and reverse intersystem crossing, respectively.

PL Decay of 4CzIPN

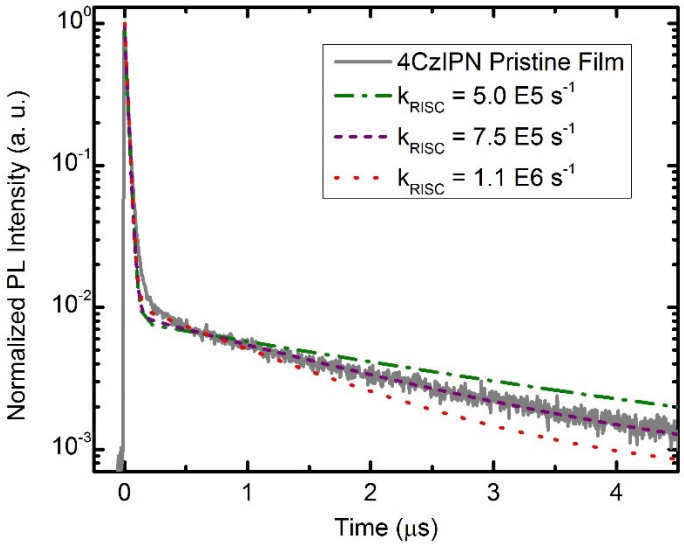

Figure S14: Calculated PL decays for a neat 4CzIPN film, with $k_{ISC} = 1.14 \times 10^7$ s^{-1}, compared to the experimentally measured PL decay. Within the theoretical plots the only parameter that changes is k_{RISC}.

	4CzIPN	
	Theoretical	**Experimental**
ΔE_{ST} (meV)	60 (average) 17 (most probable)	42
k_{ISC} (s^{-1}) uncorrected	1.14 x 10^7	1.14 x 10^7
k_{RISC} (s^{-1}) uncorrected	1.13 x 10^6	7.50 x 10^5
k_{ISC} (s^{-1}) corrected	2.60 x 10^6	2.60 x 10^6
k_{RISC} (s^{-1}) corrected	6.60 x 10^5	5.90 x 10^5

Table S4: Comparison between experimental ΔE_{ST}, (reverse) intersystem crossing [(R)ISC] rates and calculated ones, either considering polaronic effects (corrected) or not (uncorrected) in the evaluation of the spin-orbit coupling.

PL Decay of 2CzPN

We observed that 2CzPN does not exhibit a biexponential fluorescence decay, contrary to what is expected for TADF materials. In fact, the delayed component of fluorescence for 2CzPN was best described by a stretched exponential, as shown in Figure S15. The first time point in the PL decay was removed before normalizing the data so that only the delayed component of fluorescence is shown in Figure S15. The fitted function is given by:

$$\mathrm{I(t)} = y_0 + \mathrm{A}\exp(-(k_{stretch}t)^{\beta}) \qquad (S19)$$

where I(t) is the intensity of fluorescence, y_0 is the baseline (0.03), A is the amplitude (1.0), $k_{stretch}$ is the rate-constant of the decay (1.3 x 10^3 s^{-1}), and β is the stretching exponent (0.4). We found that the PL decay is independent of excitation intensity (varied by over 2 orders of magnitude), which excludes exciton-exciton interactions as a cause for this unexpected decay behavior. The PL decay of 2CzPN was also measured when it was diluted in a polystyrene matrix (98% polystyrene by weight), which suggests that the stretched exponential decay is also not a result of intermolecular interactions of 2CzPN. We performed differential scanning calorimetry (DSC) on our first batch of 2CzPN and detected a trace amount of impurity (not noticeable by mass spectrometry (MS) or proton nuclear magnetic resonance (HNMR) experiments). Our second batch gave clean results by DSC, MS, and HNMR, but the delayed component of the PL was still best described by a stretched exponential (shown in Figure S15). It is important to note that the yield of 2CzPN synthesis is very low (approximately 10%), whereas the synthesis

of 4CzIPN is much more ideal (yield of approximately 90%). Thus, it seems likely that 2CzPN has an impurity which is very difficult to remove and is the cause behind the observed stretched exponential decay.

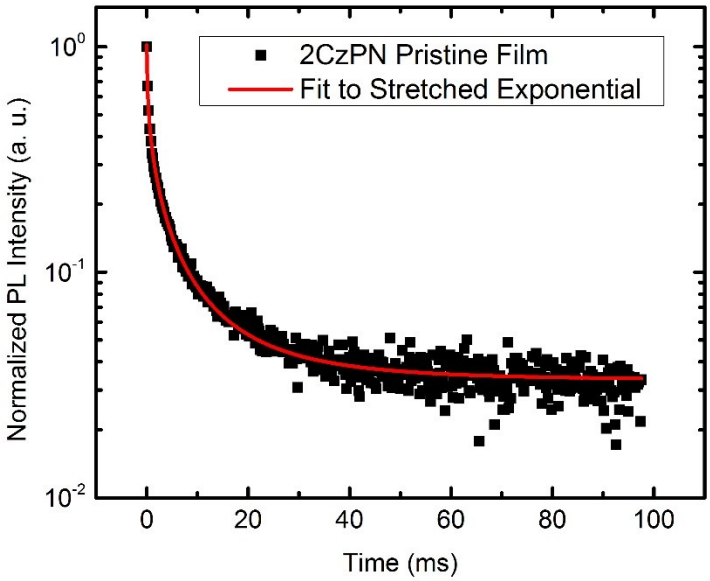

Figure S15: PL decay of 2CzPN and a fit to a stretched exponential function.

References

[1] M. Moral, W.-J. Son, J. C. Sancho-García, Y. Olivier, and L. Muccioli, J. Chem. Theory Comput. **11**, (2015).

[2] C. Adamo and V. Barone, J. Chem. Phys. **110**, 6158 (1999).

[3] M. Moral, L. Muccioli, W. J. Son, Y. Olivier, and J. C. Sancho-García, J. Chem. Theory Comput. **11**, 168 (2015).

[4] E. van Lenthe, A. Ehlers, and E. Baerends, J. Chem. Phys. **110**, 8943 (1999).

[5] F. Wang and T. Ziegler, J. Chem. Phys. **123**, 154102 (2005).

[6] E. Y. Li, T. Jiang, Y. Chi, P.-T. Chou, E. Yu-Tzu Li, T. Jiang, Y. Chi, and P.-T. Chou, Phys. Chem. Chem. Phys. **16**, 26184 (2014).

[7] H. Uoyama, K. Goushi, K. Shizu, H. Nomura, and C. Adachi, Nature **492**, 234 (2012).

[8] C. Baleizão and M. N. Berberan-Santos, J. Chem. Phys. **126**, 204510 (2007).

[9] J. Yguerabide and M. Burton, J. Chem. Phys. **37**, 1757 (1962).

[10] X. Cai, X. Li, G. Xie, Z. He, K. Gao, K. Liu, D. Chen, Y. Cao, and S.-J. Su, Chem. Sci. **7**, 4264 (2016).

[11] Y. Tao, K. Yuan, T. Chen, P. Xu, H. Li, R. Chen, C. Zheng, L. Zhang, and W. Huang, Adv. Mater. **26**, 7931 (2014).

[12] F. B. Dias, K. N. Bourdakos, V. Jankus, K. C. Moss, K. T. Kamtekar, V. Bhalla, J. Santos, M. R. Bryce, and A. P. Monkman, Adv. Mater. **25**, 3707 (2013).

[13] T. Nakagawa, S.-Y. Ku, K.-T. Wong, and C. Adachi, Chem. Commun. **48**, 9580 (2012).